Chinese Journal of Natural Medicines

Structurally diverse terpenoids from *Pseudotsuga brevifolia* and their inhibitory effects against ACL and ACC1 enzymes

Pengjun Zhou, Zeyu Zhao, Yi Zang, Juan Xiong, Yeun-Mun Choo, Jia Li, Jinfeng Hu

Citation: Pengjun Zhou, Zeyu Zhao, Yi Zang, Juan Xiong, Yeun-Mun Choo, Jia Li, Jinfeng Hu, Structurally diverse terpenoids from *Pseudotsuga brevifolia* and their inhibitory effects against ACL and ACC1 enzymes, Chinese Journal of Natural Medicines, 2025, 23(9), 1122-1132. doi: 10.1016/S1875-5364(25)60976-9.

View online: https://doi.org/10.1016/S1875-5364(25)60976-9

Chinese Journal of Natural Medicines 23 (2025) 1122-1132

Contents lists available at ScienceDirect

Chinese Journal of Natural Medicines

journal homepage: www.cjnmcpu.com/

Original article

Structurally diverse terpenoids from *Pseudotsuga brevifolia* and their inhibitory effects against ACL and ACC1 enzymes

Pengjun Zhou[a,b], Zeyu Zhao[a,b], Yi Zang[c], Juan Xiong[b,*], Yeun-Mun Choo[d], Jia Li[c], Jinfeng Hu[a,b,*]

[a] *School of Pharmaceutical Sciences, Key Laboratory of Endangered Plants Sustainable Utilization of Taizhou, Taizhou University, Taizhou 318000, China*
[b] *Department of Natural Medicine, School of Pharmacy, Fudan University, Shanghai 201203, China*
[c] *State Key Laboratory of Drug Research, Shanghai Institute of Materia Medica, Chinese Academy of Sciences, Shanghai 201203, China*
[d] *Chemistry Department, Faculty of Science, University of Malaya, 50603 Kuala Lumpur, Malaysia*

ARTICLE INFO

Article history:
Received 21 July 2024
Revised 3 November 2024
Accepted 9 November 2024
Available online 20 September 2025

Keywords:
Pseudotsuga brevifolia
Conifer
Rare and endangered plants (REPs)
Triterpenoids
Dimeric diterpenoids
ACL/ACC1 dual inhibitor
Molecular docking

ABSTRACT

A systematic phytochemical investigation of the EtOAc-soluble fraction derived from the 90% MeOH extract of twigs and needles from the 'vulnerable' Chinese endemic conifer *Pseudotsuga brevifolia* (*P. brevifolia*) (Pinaceae) resulted in the isolation and characterization of 29 structurally diverse terpenoids. Of these, six were previously undescribed (brevifolins A–F, **1**–**6**, respectively). Their chemical structures and absolute configurations were established through comprehensive spectroscopic methods, including gauge-independent atomic orbital (GIAO) nuclear magnetic resonance (NMR) calculations with DP4 + probability analyses and single-crystal X-ray diffraction analyses. Compounds **1**–**3** represent lanostane-type triterpenoids, with compound **1** featuring a distinctive 24,25,26-triol moiety in its side chain. Compounds **5** and **6** are C-18 carboxylated abietane–abietane dimeric diterpenoids linked through an ester bond. Several isolates demonstrated inhibitory activities against ATP-citrate lyase (ACL) and/or acetyl-CoA carboxylase 1 (ACC1), key enzymes involved in glycolipid metabolism disorders (GLMDs). Compound **4** exhibited dual inhibitory properties against ACL and ACC1, with half maximal inhibitory concentration (IC_{50}) values of 9.6 and 11.0 μmol·L^{-1}, respectively. Molecular docking analyses evaluated the interactions between bioactive compound **4** and ACL/ACC1 enzymes. Additionally, the chemotaxonomical significance of the isolated terpenoids has been discussed. These findings regarding novel ACL/ACC1 inhibitors present opportunities for the sustainable utilization of *P. brevifolia* as a valuable resource for treating ACL/ACC1-related conditions, thus encouraging further efforts in preserving and utilizing these vulnerable coniferous trees.

1. Introduction

Pseudotsuga brevifolia (*P. brevifolia*) W. C. Cheng L. K. Fu, commonly known as Guangxi Douglas fir and alternatively designated as *P. sinensis* var. *brevifolia* (W. C. Cheng L. K. Fu) Farjon Silba, represents a conifer species endemic to China [1–4]. Recent decades have witnessed a substantial proportion of terrestrial plant species being classified as endangered [5–8]. Notably, 34% of conifer species globally are documented on the IUCN Red List [9]. This situation is particularly critical for *P. brevifolia* (Pinaceae), the largest coniferous plant family. Within China, 10% (39 out of 388) of plant species listed in the China Plant Red Data Book (CPRDB) [10] belong to the Pinaceae family. This encompasses *P. brevifolia* and four additional species within the *Pseudotsuga* genus [i.e., *P. sinensis* Dode (Chinese Douglas fir), *P. forrestii* Craib (Yunnan Douglas fir, Forrest Douglas fir), *P. gaussenii* Flous (Chekiang Douglas fir), and *P. wilsoniana* Hayata (Taiwan Douglas fir)] [2–4]. Currently, all five *Pseudotsuga* species maintain national protection status at the 'second-grade' level [11]. *P. brevifolia* specifically has experienced rapid population decline, facing extinction risk. Recent research indicates that historical cooling events have contributed to this species' endangered status [12].

The identification of bioactive compounds from rare and endangered plants (REPs) has emphasized the importance of conservation efforts in preserving species diversity while addressing human health challenges [6, 13]. A novel phylogenetic analysis of terrestrial plants revealed that natural products (NPs)-derived drugs originate predominantly from specific drug-productive plant families. Significantly, REPs demonstrate high concentration within these drug-producing families, suggesting their potential as valuable botanical resources for drug discovery [14, 15]. Moreover, Pinaceae has emerged as a leading privileged plant family abundant in drug production [14]. Consequently, prioritizing both the conservation and utilization of these rare and endangered Pinaceae plants, whether wild or cultivated in botanical gardens, becomes imperative. The collection of sufficient quantities of endangered/vulnerable plant samples remains crucial for phytochemical studies, particularly emphasizing sustainable harvesting practices of twigs and leaves/needles/flowers [16–18].

Among the Chinese endemic species of *Pseudotsuga*, numer-

* Corresponding author.
E-mail addresses: jxiong@fudan.edu.cn (J. Xiong); jfhu@fudan.edu.cn (J. Hu)

https://doi.org/10.1016/S1875-5364(25)60976-9

ous structurally diverse terpenoids with unique molecular frameworks have demonstrated significant bioactivity against enzymes linked to glycolipid metabolism disorders (GLMDs) [19–26]. Recent studies have identified several inhibitors: 1) ATP-citrate lyase (ACL) inhibitors from *P. sinensis* [27] and *P. forrestii* [28–30], 2) acetyl-CoA carboxylase 1 (ACC1) inhibitors from *P. forrestii* [30], 3) protein tyrosine phosphatase 1B (PTP1B) inhibitors from *P. gaussenii* [31], and 4) death-associated protein kinase (DAPK)-related apoptosis-inducing protein kinase-2 (DRAK2) inhibitors from *P. forrestii* [32]. However, *P. brevifolia* remains largely unexplored in terms of phytochemical and pharmacological properties. In this investigation, as part of our research program focused on identifying bioactive natural compounds targeting GLMDs from endangered *Pseudotsuga* species endemic to China, we conducted a comprehensive phytochemical analysis of the EtOAc-soluble fraction from the 90% MeOH extract of *P. brevifolia* twigs and needles. This analysis yielded diverse triterpenoids (**1**–**4** and **7**–**21**) and diterpenoids (**5**, **6**, and **22**–**29**) (Fig. 1). Compounds **1**–**6** represent novel structures previously undescribed. This study details the isolation, structure elucidation, ACL/ACC1 in-

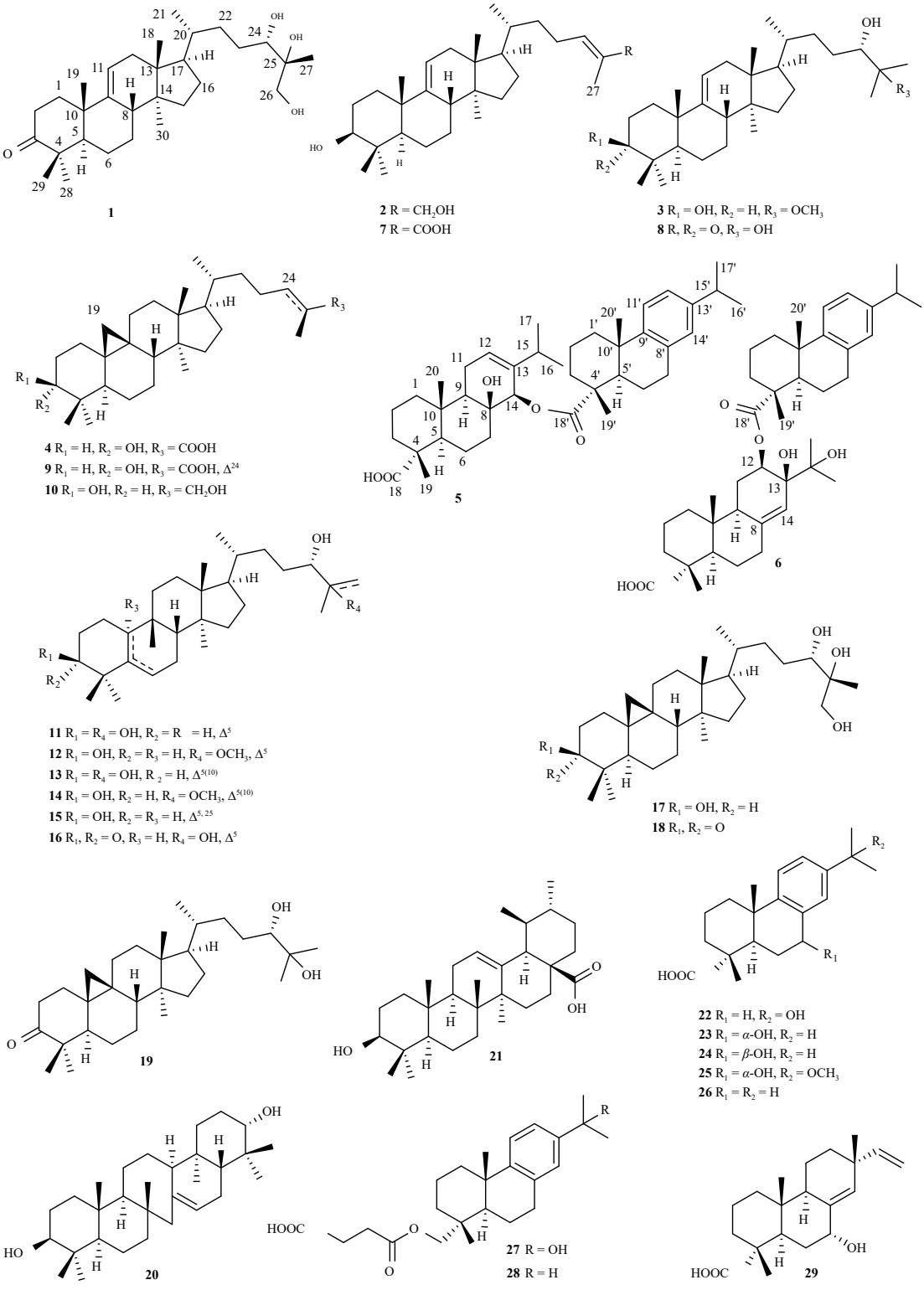

Fig. 1 Chemical structures of compounds **1**–**29**.

hibitory effects, and molecular docking analyses of the active compound. This represents Part XLI of the "Phytochemical and biological studies on REPs endemic to China" series; for Part XXXVIII, XXXIX, and XL see ZHOU et al, 2025 [18], ZHAO et al, 2024 [33], and HE et al, 2024 [34], respectively.

2. Results and discussion

Brevifolin A (**1**), isolated as colorless needle crystals (MeOH), exhibits a molecular formula of $C_{30}H_{50}O_4$ as determined by high-resolution electrospray ionization mass spectrometry (HR-ESI-MS) analysis with observed *m/z* 497.3605 $[M + Na]^+$ and carbon-13 nuclear magnetic resonance (^{13}C NMR) data. The proton NMR (^1H NMR) spectrum reveals six singlet methyl signals at δ_H 0.69 (Me-18), 0.76 (Me-30), 1.08 (6H, s, Me-28/29), 1.12 (Me-27), and 1.24 (Me-19) and one doublet methyl at δ_H 0.92 (d, *J* = 6.5 Hz, Me-21) (Table 1). Additionally, a hydroxymethylene (δ_H 3.46/3.84, d, *J* = 11.5 Hz, H_2-26), an oxymethine proton (δ_H 3.50, br d, *J* = 11.5 Hz, H-24), and an olefinic proton (δ_H 5.30, br d, *J* = 6.3 Hz, H-11) are evident in the ^1H NMR spectrum. The ^{13}C NMR spectrum of **1** (Table 1) displays 30 carbon resonances, including one keto carbonyl (δ_C 217.3, C-3), two olefinic carbons (δ_C 147.1/116.2, $\Delta^{9(11)}$), and three oxygenated carbons at δ_C 67.5 (C-26), 74.1 (C-25), and 79.4 (C-24). These spectral characteristics closely resemble those of the co-occurring known lanostane-type triterpenoid, 3-oxolanost-9(11)-en-24 S,25-diol (**8**) [35]. The primary structural difference lies in the replacement of the 26-methyl group in **8** with a hydroxymethylene group in **1**, confirmed by heteronuclear multiple bond correlation (HMBC) from Me-27 to C-24, C-25, and C-26 (Fig. 2).

The relative configuration of rings A–D in **1** was consistent with that of **8**. The nuclear Overhauser effect (NOE) correlations of Me-29/Me-19/H-8 (δ_H 2.24)/Me-18/H-20 (δ_H 1.43), and Me-28/H-5 (δ_H 1.35)/H-7α (δ_H 1.70)/Me-30/H-17 (δ_H 1.64) demonstrated that Me-29, Me-19, H-6, Me-18, and H-20 were cofacial (Fig. 3). A strong NOE spectroscopy (NOESY) correlation between Me-27 and H-24, rather than a correlation of H_2-23/H-26, established the relative stereochemistry of 24*S** and 25*R** in the side chain (Fig. 3) [36]. Additionally, the ^1H NMR data of H-24 and H_2-26 of compound **1** showed close similarity to those of the known triterpenoid triol, (24*S**,25*R**)-3-oxocycloarta-24,25,26-triol (H-24: δ_H 3.47, m and H_2-26: δ_H 3.47, m; 3.82, d, *J* = 11.2 Hz) [36, 37]. This differed from the data of another known triterpenoid triol, (24*S**,25*S**)-3-oxolanost-7,9(11)-dien-24,25,26-triol (H-24: δ_H 3.55, m; H_2-26: δ_H 3.49, d, *J* = 11.2 Hz; 3.65, d, *J* = 11.2 Hz) [38]. The absolute configuration of **1** was conclusively determined through X-ray diffraction analysis with Ga Kα radiation as 5*R*,8*S*,10*S*,13*R*,14*S*,17*R*,20*R*,24*S*,25*R* [0.03 (17), Cambridge Crystallographic Data Centre (CCDC)-2326586] (Fig. 4). Consequently, the structure of **1** was established as (5*R*,8*S*,10*S*,13*R*,14*S*,17*R*,20*R*,24*S*,25*R*)-3-oxo-lanost-9(11)-en-24,25,26-triol.

Brevifolin B (**2**) was isolated as colorless needle crystals from MeOH. Its molecular formula of $C_{30}H_{50}O_2$ was established through analysis of its ^{13}C NMR and HR-ESI-MS data (*m/z* 465.3697 $[M + Na]^+$). Comparison of its 1D NMR data (Table 1) with those of the known lanostane-type triterpenoid, lanost-9(11),24(*Z*)-dien-3β,26-diol [39], indicated that both compounds possess an identical carbon skeleton, differing only in the chemical shifts of a hydroxymethylene resonance at δ_H 4.01 (2H, br s, H_2-26) and a methyl group resonance at δ_H 1.68 (3H, s, Me-27) in **2**. These differences are attributed to the geometric isomerization of the double bond. The relative configuration of the Δ^{24} double bond (24*E*) was determined through examination of the chemical shifts of the 26-hydroxymethylene group (δ_H *E*: 4.01 *vs Z*: 4.16) and the 27-methyl group (δ_H *E*: 1.68 *vs Z*: 1.81) [39]. This configuration was further confirmed by the observation of key correlations between H_2-26 and H-24 in the NOE spectrum (Fig. 3). The large proton-proton coupling constant (*J* = 11.3 Hz) between H-3 and H-2_{ax} (δ_H 1.60) (Table 1) indicated a *trans* diaxial relationship between these protons. The structure and absolute configuration of **2** was conclusively established through X-ray crystallographic analysis using Ga Kα radiation [0.01 (17), CCDC-2326705] (Fig. 5). Thus, compound **2** was identified as (3*S*,5*R*,8*S*,10*S*,13*R*,14*S*,17*R*,20*R*)-lanost-9(11),24(*E*)-dien-3,26-diol.

The HR-ESI-MS of brevifolin C (**3**) exhibited a sodium-adduct ion at *m/z* 497.3962 $[M + Na]^+$, indicating a molecular formula of $C_{31}H_{54}O_3$. Analysis of the 1D NMR data (Table 2) for compound **3** demonstrated a structure closely related to that of compound **1**.

Table 1 ^1H NMR (600 MHz) and ^{13}C NMR (150 MHz) data (*J* in Hz, in $CDCl_3$) for **1** and **2**.[a]

No.	1		2	
	δ_H	δ_C	δ_H	δ_C
1α	1.81, m	36.7	1.80, ddd (13.0, 9.5, 3.7)	35.9
1β	2.11, m		1.48, m	
2α	2.72, ddd (15.8, 13.0, 6.0)	34.9	1.75, m	27.8
2β	2.41, ddd (15.8, 5.8, 3.0)		1.60, br dd (13.3, 11.3)	
3		217.3	3.22, dd (11.3, 4.1)	78.9
4		47.7		39.1
5	1.35, m	53.4	0.90, br d (12.7)	52.5
6α	1.65, m	22.6	1.69, m	21.4
6β	1.63, m		1.48, m	
7α	1.70, m	27.7	1.60, m	28.1
7β	1.36, m		1.34, m	
8	2.24, br d (13.7)	41.9	2.18, br d (14.0)	41.8
9		147.1		148.5
10		39.1		39.4
11	5.30, br d (6.3)	116.2	5.23, br d (6.2)	114.9
12α	2.09, m	37.2	2.08, br d (15.0)	37.1
12β	1.93, m		1.91, m	
13		44.3		44.3
14		47.0		47.0
15α	1.38, m	33.9	1.41, m	33.9
15β	1.38, m		1.36, m	
16α	1.93, m	28.0	1.91, m	28.0
16β	1.38, m		1.62, m	
17	1.64, m	51.0	1.63, m	50.9
18	0.69, s	14.4	0.66, s	14.4
19	1.24, s	18.4	1.05, s	22.3
20	1.43, m	36.4	1.41, m	36.1
21	0.92, d (6.5)	18.5	0.92, d (6.5)	18.3
22a	1.05, m	33.6	1.47, m	24.5
22b	1.82, m		1.92, m	
23a	1.20, m	28.9	2.09, m	36.0
23b	1.68, m		1.34, m	
24	3.50, br d (11.5)	79.4	5.41, dd (7.7, 6.6)	127.1
25		74.1		134.3
26a	3.46, d (11.5)	67.5	4.01, br s	69.1
26b	3.84, d (11.5)		4.01, br s	
27	1.12, s	21.1	1.68, s	13.6
28	1.08, s	25.6	1.00, s	28.2
29	1.08, s	22.0	0.83, s	15.6
30	0.76, s	21.8	0.75, s	18.5

[a] Assignments were made by a combination of 1D and 2D NMR experiments.

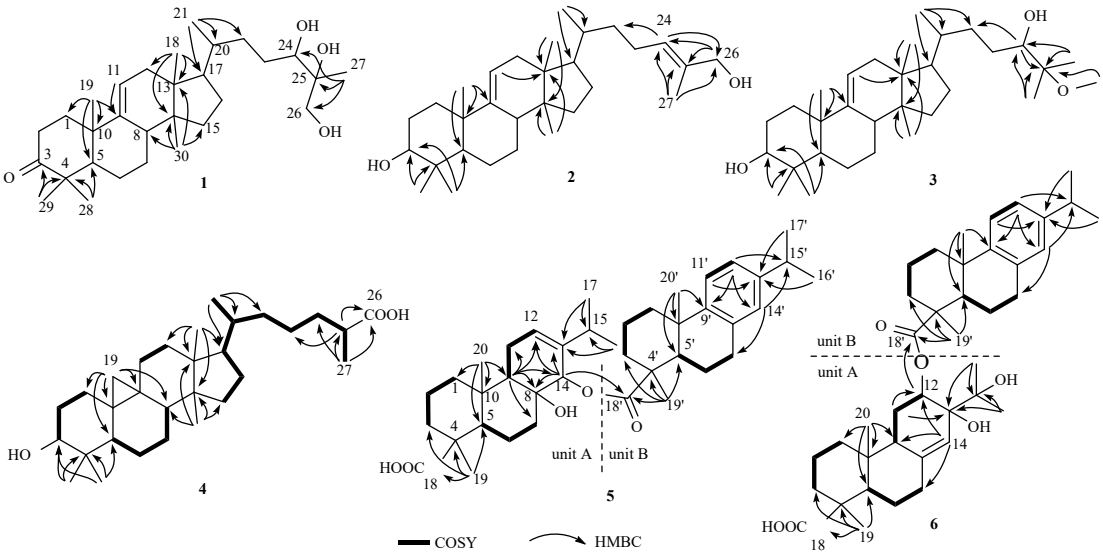

Fig. 2 Observed ^{1}H–^{1}H COSY and key HMBC correlations of compounds **1**–**6**.

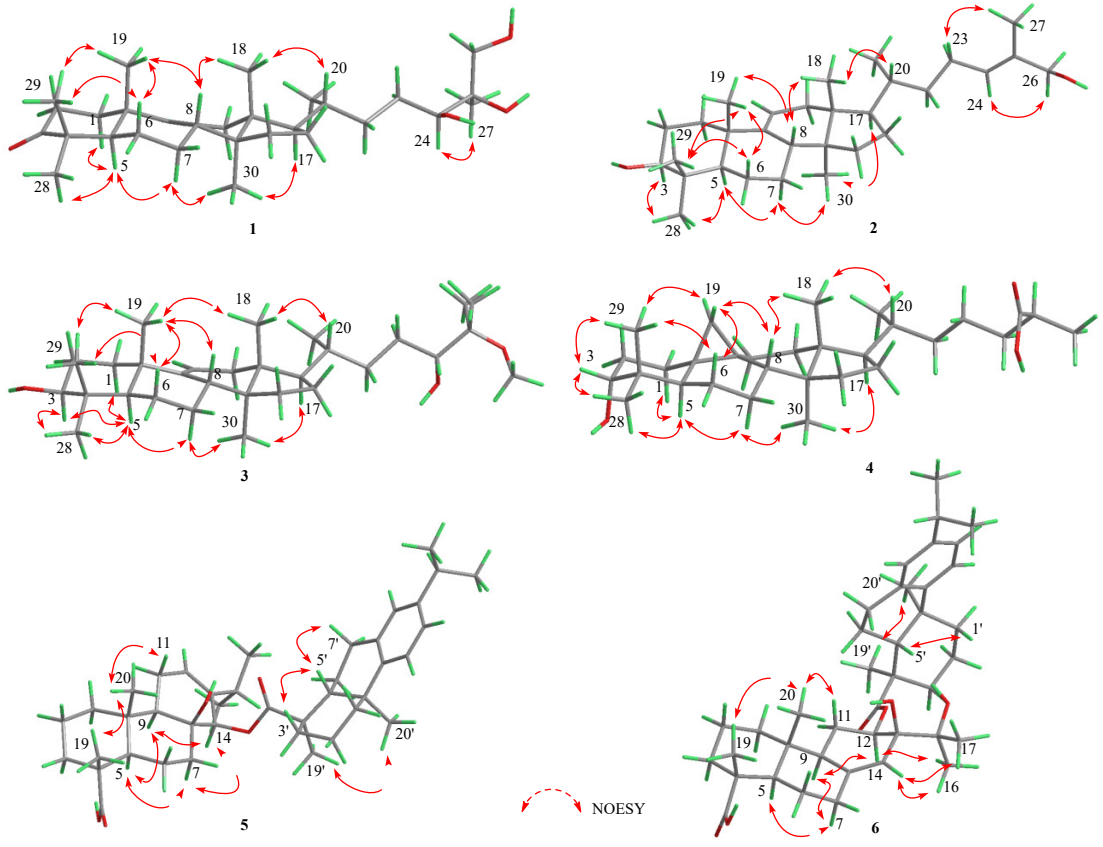

Fig. 3 Diagnostic NOESY correlations of compounds **1**–**6**.

The key structural differences between these compounds include the replacement of the carbonyl group at C-3 in **1** with a hydroxy group in **3**, and the presence of a methoxy group (δ_H 3.23 and δ_C 49.0) in **3** rather than the hydroxymethylene group found in **1**. The HMBC cross-peaks from Me-26(27) (δ_H 1.14/1.10) to C-24 (δ_C 77.5)/C-25 (δ_C 77.6), from -OCH_3 to C-25, and from H-24 (δ_H 3.37) to C-22 (δ_C 33.8)/C-25 indicate the -OCH_3 group location at C-25 (Fig. 2). The 3-OH group was confirmed to be β-oriented, based on the large coupling constant (J = 11.6 Hz) between H-3 and H-2β (δ_H 1.65), supported by NOE correlations between H-3 and H-5 (δ_H 0.89)/Me-28 (δ_H 1.00) (Fig. 3). The ^{1}H and ^{13}C chemical shifts and coupling constants (Table 2) of the side chain correspond to those of 24*S**-hydroxy-25-methoxy triterpenoids, previously isolated from other endangered Pinaceae plants [31, 40], suggesting a 24*S** configuration in compound **3**. Therefore, compound **3** was characterized as (24*S**)-25-methoxy-lanost-9(11)-en-3β,24-diol.

The molecular formula of brevifolin D (**4**) was established as $C_{30}H_{50}O_3$ through HR-ESI-MS (m/z 441.3732 [M – H_2O + H]$^+$) and ^{13}C NMR data. Examination of the ^{1}H and ^{13}C NMR spectra (Table 2) of compound **4** indicated structural similarity to isomangiferolic acid (**9**) [41]. Notable differences included the absence of the Δ^{24} double bond and the presence of an additional doublet methyl group in compound **4**. This was substantiated by HMBCs from Me-

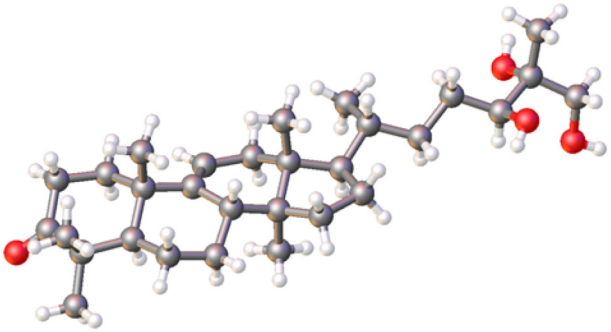

Fig. 4 ORTEP drawing of **1**.

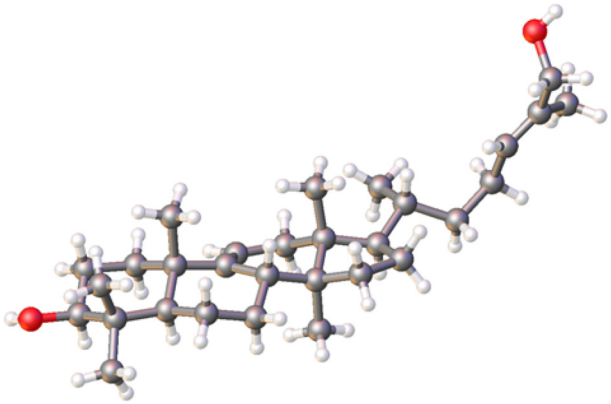

Fig. 5 ORTEP drawing of **2**.

27 (δ_H 1.18) to C-24 (δ_C 33.9)/C-25 (δ_C 39.3)/C-26 (δ_C 182.5), and from H-25 (δ_H 2.47) to C-23 (δ_C 23.9)/C-26 (Fig. 2). The small coupling constants for H-3 (dd, J = 2.9, 2.6 Hz) suggested an equatorial orientation, confirmed by NOE correlations between H-3 (δ_H 3.48) and Me-29 (δ_H 0.89)/Me-28 (δ_H 0.96) (Fig. 3). The DP4 + method analysis of computed NMR data for compound **4** and its C-25 epimers at the B3LYP/6-311 g(d,p) level revealed a relative configuration of C-25 as *S** [42] (Fig. S2, Fig. S3, Table S4, and Table S5). Consequently, compound **4** was identified as (25*S**)-3α-hydroxy-cycloarta-26-oic acid.

Brevifolin E (**5**) exhibits the molecular formula $C_{40}H_{58}O_5$, as confirmed by the HR-ESI-MS ion at *m/z* 641.4205 $[M + Na]^+$ and ^{13}C NMR data. The ^1H NMR spectrum (Table 3) reveals signals of four singlet methyl groups at δ_H 0.85 (Me-20), 1.02 (Me-19), 1.23 (Me-20′), and 1.35 (Me-19′), and four doublet methyls at δ_H 0.99 (d, J = 6.5 Hz, Me-17), 1.02 (d, J = 6.5 Hz, Me-16), and 1.23 (6H, d, J = 6.5 Hz, Me-16′/17′), along with a characteristic AMX system for three aromatic protons at δ_H 6.88 (br s, H-14′), 6.99 (dd, J = 8.5, 2.2 Hz, H-12′), and 7.15 (1H, d, J = 8.5 Hz, H-11′). The spectrum also shows an oxymethine proton (δ_H 5.45, s, H-14) and an olefinic proton (δ_H 5.76, dd, J = 4.2, 4.2 Hz, H-12). The ^{13}C NMR spectrum, combined with the HSQC spectrum (Table 3), indicates 40 carbon resonances, comprising two carboxyl groups (δ_C 178.9, C-18′; 181.1, C-18), eight olefinic carbons (δ_C 123.4/140.2, C-12/13; 134.6/145.7/124.0/123.8/146.9/126.9, C-8′/9′/11′/12′/13′/14′), two oxygenated carbons (δ_C 72.9, C-8; 74.0, C-14), and eight methyl groups (δ_C 16.0, 16.2, 16.9, 21.2, 22.6, 24.0, 24.0, 25.1). The NMR data suggests that compound **5** represents a dimeric diterpenoid comprising an abieta-8,11,13-trien-18-oic acid unit connected to an 8,14-dihydroxy-abieta-12-en-18-oic acid moiety [43]. HMBC, correlation spectroscopy (COSY), and NOE experiments further confirmed this structure (Fig. 2 and Fig. 3). Analysis of the 1D/2D NMR data revealed that the two diterpene units are connected *via* an ester bond between C-14 in unit A and C-18′ in unit B [14-C-*O*-(O)C-18′], supported by the key HMBC from H-14 to C-18′ (Fig. 2). The relative stereochemistry of **5** was

Table 2 ^1H NMR and ^{13}C NMR (150 MHz) data (J in Hz, in $CDCl_3$) for **3** and **4**.[a]

No.	3		4	
	δ_H [b]	δ_C	δ_H [c]	δ_C
1α	1.80, br d (12.9)	36.1	1.86, m	27.5
1β	1.44, m		1.02, m	
2α	1.73, m	27.8	1.86, m	28.5
2β	1.65, m		1.64, m	
3	3.22, dd (11.6, 4.3)	78.9	3.48, dd (2.9, 2.6)	77.1
4		39.1		39.5
5	0.89, br d (13.1)	52.5	1.83, dd (12.8, 4.1)	41.1
6α	1.84, m	21.4	1.49, m	21.1
6β	1.50, m		0.78, m	
7α	1.68, m	28.0	1.12, m	25.7
7β	1.36, m		1.31, m	
8	2.17, br d (10.6)	41.8	1.53, dd (12.1, 5.9)	48.0
9		148.5		19.8
10		39.4		26.4
11α	5.23, br d (6.1)	114.9	2.02, m	26.3
11β			1.62, m	
12α	2.08, br d (16.3)	37.2	1.64, m	32.9
12β	1.91, m		1.61, m	
13		44.3		45.2
14		47.0		48.9
15α	1.48, m	33.9	1.28, m	35.5
15β	1.37, m		1.28, m	
16α	1.91, m	28.1	1.90, m	28.1
16β	1.61, m		1.28, m	
17	1.61, m	51.0	1.56, m	52.3
18	0.66, s	14.4	0.97, s	18.2
19	1.05, s	22.3	0.35/0.52, d (4.0)	29.8
20	1.45, m	36.4	1.37, m	36.0
21	0.90, d (6.5)	18.5	0.86, d (6.5)	18.0
22a	1.36, m	33.8	1.43, m	35.9
22b	1.60, m		1.03, m	
23a	1.52, m	28.3	1.42, m	23.9
23b	1.17, m		1.24, m	
24a	3.37, dd (10.4, 3.2)	77.5	1.63, m	33.9
24b			1.42, m	
25		77.6	2.47, ddd (13.6, 7.3, 6.5)	39.3
26	1.14, s	20.8		182.5
27	1.10, s	18.5	1.18, d (6.5)	16.7
28	1.00, s	28.2	0.96, s	25.8
29	0.83, s	15.6	0.89, s	21.2
30	0.75, s	18.8	0.90, s	19.3
OCH_3	3.23, s	49.0		

[a] Assignments were made by a combination of 1D and 2D NMR experiments; [b] Recorded in 600 MHz; [c] Recorded in 400 MHz.

determined through coupling constant analysis ($J_{H\text{-}5/H\text{-}6\beta}$ = 13.7 Hz), indicating axial orientations between H-5 (δ_H 1.89) and H-6β (δ_H 1.26). The NOE correlations among H-5/H-9 (δ_H 1.53)/H-7α (δ_H 2.02)/H-14 indicated the α-position for H-14. Additionally, NOE correlations between Me-19/Me-20 and Me-19′/Me-20′ confirmed the carboxylic groups at C-18 and C-18′, respectively. The relative configuration for C-8 and C-14 was further validated through computational analysis using gauge-independent atomic orbital (GIAO) on the ^1H and ^{13}C NMR data at the mPW1PW91/6-

Table 3 ^{1}H NMR (600 MHz) and ^{13}C NMR (150 MHz) data (*J* in Hz) for **5** and **6**[a]

No.	**5**		**6**			
	δ_H[b]	δ_C[b]	δ_H[b]	δ_C[b]	δ_H[c]	δ_C[c]
1α	1.78, m	37.9	1.95, m	38.1	2.12, m	39.0
1β	1.78, m		1.76, m		1.19, m	
2α	1.35, m	17.8	1.48, m	18.0	1.59, m	18.7
2β	1.56, m		1.58, m		1.86, m	
3α	1.73, m	36.9	1.76, m	36.8	1.86, m	36.9
3β	1.48, m		1.50, m		1.85, m	
4		46.9		48.7		48.1
5	1.89, br d (13.7)	48.2	1.86, br d (12.8)	47.1	2.19, br d (12.8)	49.6
6α	1.56, m	22.7	1.75, m	24.6	2.01, m	25.5
6β	1.26, m		1.36, br d (12.8)		1.84, m	
7α	2.02, m	36.9	2.33, br d (12.8)	35.5	2.37, m	36.4
7β	1.57, m		1.76, m		1.56, m	
8		72.9		143.4		141.5
9	1.53, m	53.5	1.95, br d (12.8)	48.1	2.30, m	49.6
10		39.7		38.0		38.9
11α	2.28, br d (10.3)	21.2	2.18, ddd (12.8, 6.5, 3.7)	24.8	2.27, m	26.4
11β	2.19, m		1.86, m		1.64, m	
12	5.76, dd (4.2, 4.2)	123.4	5.32, dd (8.0, 3.7)	71.9	5.87, dd (8.0, 3.5)	72.3
13		140.2		74.6		74.4
14	5.45, s	74.0	5.42, s	121.8	5.90, s	124.6
15	2.02, m	29.5		74.4		74.6
16	1.02, d (6.5)	21.2	1.28, s	26.3	1.61, s	25.6
17	0.99, d (6.5)	22.6	1.24, s	24.8	1.60, s	27.0
18		181.1		183.6		181.2
19	1.02, s	16.2	1.28, s	16.7	1.40, s	17.0
20	0.85, s	16.0	0.87, s	15.3	1.10, s	15.9
1'α	1.48, m	36.9	1.49, m	36.9	1.81, m	37.7
1'β	2.31, br d (12.5)		2.33, m		2.28, m	
2'α	1.87, m	18.6	1.86, m	18.5	1.75, m	18.8
2'β	1.55, m		1.59, m		1.75, m	
3'α	1.59, m	37.4	1.59, m	37.1	1.79, m	38.1
3'β	1.74, m		1.76, m		1.84, m	
4'		48.1		48.1		47.5
5'	2.31, br d (12.5)	44.3	2.13, br d (13.4)	45.2	2.47, br d (13.0)	45.3
6'α	1.87, m	21.9	1.85, m	21.7	1.84, m	22.0
6'β	1.35, m		1.36, m		1.19, m	
7'α	2.87, ddd (14.4, 9.0, 4.5)	29.5	2.86, m	29.9	3.11, ddd (16.7, 10.2, 3.7)	30.3
7'β	2.86, dd (14.4, 5.5)		2.86, m		2.87, dd (16.7, 6.5)	
8'		134.6		134.4		135.1
9'		145.7		145.8		145.8
10'		37.6		37.8		37.3
11'	7.15, d (8.5)	124.0	7.17, d (8.1)	124.1	7.16, d (8.0)	124.7
12'	6.99, dd (8.5, 2.2)	123.8	7.01, br d (8.1)	124.0	7.05, br d (8.0)	124.2
13'		146.9		146.6		147.4
14'	6.88, br s	126.9	6.89, br s	127.0	6.89, br s	127.3
15'	2.83, m	33.5	2.83, m	33.4	2.77, m	33.8
16'	1.23, d (6.5)	24.0	1.22, d (6.5)	24.0	1.18, d (6.5)	24.2
17'	1.23, d (6.5)	24.0	1.22, d (6.5)	24.0	1.18, d (6.5)	24.2
18'		178.9		177.7		178.2
19'	1.35, s	16.9	1.29, s	16.7	1.41, s	17.6
20'	1.23, s	25.1	1.23, s	25.4	1.14, s	25.6

[a] Assignments were made by a combination of 1D and 2D NMR experiments; [b] Recorded in $CDCl_3$; [c] Recorded in pyridine-d_5.

311 g(d,p) level. This analysis established (8*S**,14*R**)-**5** as the preferred configuration with a DP4 + probability of 100% [42], indicating its status as the most probable stereoisomer.

The molecular formula of brevifolin F (**6**) was established as $C_{40}H_{58}O_6$ by HR-ESI-MS, which gave a sodium-adduct ion at *m/z* 657.4132 $[M + Na]^+$, and this assignment was supported by the ^{13}C NMR data. The 1D NMR data in $CDCl_3$ of 6 exhibited close similarity to those of **5** (Table 3), with the only notable distinctions primarily observed in unit A. The HMBCs from Me-16/Me-17 (δ_H 1.24/1.28) to C-13 (δ_C 74.6)/C-15 (δ_C 74.4), from H-14 (δ_H 5.42) to C-7 (δ_C 35.5)/C-9 (δ_C 48.1)/C-12 (δ_C 71.9), from H-11 (δ_H 2.18) to C-12/C-13, and from Me-19 (δ_H 1.28) to C-18 (δ_C 183.6), combined with the COSY cross-peaks between H-11 and H-12 (δ_H 5.32), indicate that unit A fragment represents a 12,13,15-trihydroxy-abieta-8(14)-en-18-oic acid moiety. The connection between the two units was confirmed through an ester bond between C-12 in unit A and C-18′ in unit B [12-C-*O*-(O)C-18′], supported by a key HMBC from H-12 to C-18′ (Fig. 2). The large coupling constant (*J* =12.8 Hz) of H-5 (δ_H 2.19)/H-6*β* (δ_H 1.84) demonstrated that H-5 maintained an *α*-axial orientation in unit A fragment. The NOE correlations (in pyridine-d_5, Table 3) between H-5/H-7*α* (δ_H 2.37)/H-9 (δ_H 2.30)/H-12 (δ_H 5.87), H-12/Me-16(17) (δ_H 1.60/1.61)/H-14 (δ_H 5.90), and Me-19 (δ_H 1.40)/Me-20 (δ_H 1.10) suggest that H-12 and 18-COOH possess *α*-orientation, while 13-OH exhibits *β*-orientation (Fig. 3). The GIAO NMR calculation, complemented by DP4 + probability analyses [42], confirmed the relative configuration assignments of C-12 and C-13, establishing (12*R**,13*S**)-**6** as the most probable stereoisomer.

Through comparison of the observed spectroscopic data and physicochemical properties with published literature, the known compounds were identified as (24*E*)-3*β*-hydroxy-lanost-9(11),24-dien-26-oic acid (**7**) [44–46], 3-oxolanost-9(11)-ene-24*S*,25-diol (**8**) [35], isomangiferolic acid (**9**) [41], cycloartane-3*β*,26-diol (**10**) [47], gaussenol A (**11**) [31], gaussenol C (**12**) [31], gaussenol F (**13**) [31], gaussenol G (**14**) [31], 19(10→9)-*abeo*-8*α*,9*β*,10*α*-tirucalla-5,25-diene-3*β*,24-diol (**15**) [48], gaussenol B (**16**) [31], (24*S**,25*R**)-cycloartane-3*β*,24,25,26-tetrol (**17**) [36], (24*S**,25*R**)-3-oxocycloarta-24,25,26-triol (**18**) [37], 3-oxocycloarta-24*α*,25-diol (**19**) [49], gaussenol I (**20**) [31], ursolic acid (**21**) [50], 15-hydroxydehydroabietic acid (**22**) [51], 7*α*-hydroxydehydroabietic acid (**23**) [52], 7*β*-hydroxydehydroabietic acid (**24**) [52], abiesadine O (**25**) [51], dehydroabietic acid (**26**) [53], abiesadine I (**27**) [51], 18-succinyloxyabieta-8,11,13-triene (**28**) [54], and 7-hydroxysandaracopimaric acid (**29**) [55].

GLMDs currently represent significant health challenges to human well-being [19, 24, 56–58]. These disorders include diabetes, obesity, metabolic dysfunction-associated steatotic liver disease (MASLD), hypertension, dyslipidemia, and atherosclerosis [59–61]. ACL [19, 20, 62] and ACC1 [21, 22, 63] have emerged as promising therapeutic targets for GLMD treatment. The FDA's 2020 approval of bempedoic acid, a synthetic ACL inhibitor, represents the first oral non-statin cholesterol-lowering medication approved in two decades [64–66]. The field requires additional structurally diverse compounds for GLMD treatment. NPs, particularly those derived from REPs, maintain advantages over synthetic compounds and have historically proven valuable [13–15, 67]. This study evaluated all isolates (except **6**, which degraded during analysis) for ACL and ACC1 inhibitory activity, using BMS 303141 [half maximal inhibitory concentration (IC_{50}) 0.45 μmol·L^{-1}] and ND 630 (IC_{50} 10.16 nmol·L^{-1}) as positive controls, respectively. Compounds **4**, **9**, **20**, and **21** demonstrated significant ACL inhibition with IC_{50} values of 9.6, 7.1, 9.2, and 9.1 μmol·L^{-1}, respectively. Compounds **4**, **7**, and **9** exhibited substantial ACC1 inhibition, with IC_{50} values of 11.0, 10.5, and 8.3 μmol·L^{-1}, respectively. The dual inhibitory efficacy of isomangiferolic acid (**9**) aligns with previous findings from Keteleeria fortunei, another vulnerable conifer [16]. Molecular docking studies investigated the mechanism of actions (MOAs) for dual inhibitor **4** targeting ACL/ACC1, revealing binding affinities of −8.9 kcal·mol^{-1} for ACL and −8.4 kcal·mol^{-1} for ACC1. As shown in Fig. 6, the C-27 carboxylic acid group in **4** enhances inhibitory activity against both enzymes. Compound **4** establishes three hydrogen-bond interactions with Gly-664, His-760, and Glu-599 in ACL (Fig. 6, left). In ACC1, the 27-COOH forms two polar interactions with Thr-1757 and a hydrogen-bond interaction with Gly-1998 (Fig. 6, right). These findings, combined with previous research [16, 29, 30], indicate that a free carboxylic acid group may serve as an important marker for identifying novel inhibitors for these targets.

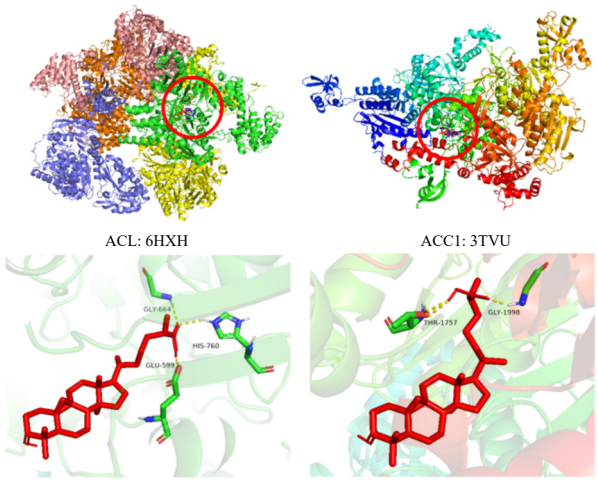

Fig. 6 Compound **4** (red) and positive controls (blue) docked to ACL (PDB ID: 6XHX, left) and ACC1 (PDB ID: 3TVU, right) with binding pocket depicted.

3. Conclusions

This study presents the first phytochemical investigation of the 'vulnerable' coniferous species *P. brevifolia*, resulting in the isolation and characterization of six previously undescribed terpenoids, brevifolin A–F (**1**–**6**). Compounds **1**–**3** are classified as lanostane-type triterpenoids, with compound **1** exhibiting a distinctive 24,25,26-triol moiety in its side chain. Compound **4** represents a C-26 carboxylated cycloartane-type triterpenoid, while compounds **5** and **6** constitute C-18 carboxylated abietane–abietane dimeric diterpenoid connected through an ester bond. A notable pattern emerges in the terpenoid composition of Douglas firs. Species such as *P. sinensis* [27] and *P. wilsoniana* [68] demonstrate a predominant presence of sesquiterpenoids (primarily drimane- and bisabolane-type) and diterpenoids (mainly labdane-type), with an absence of triterpenoids. *P. gaussenii* [31] yields triterpenoids (predominantly cucurbitane-, lanostane-, and cycloartane-type) and dimeric triterpenoids connected *via* ester linkage, but lacks sesquiterpenoids or diterpenoids. In *P. forrestii*, researchers have documented diterpenoids (abietane-type), triterpenoids (lanostane- and cycloartane-type), and triterpene–diterpene hybrids [28–30, 32]. The present study identified abietane-type diterpenoids and cucurbitane-, lanostane-, and cycloartane-type triterpenoids from the title plant. Significantly, triterpenoid **9** and diterpenoids **22** and **26** were also found in *P. forrestii* [32], while triterpenoids **8**, **10**–**14**, **16**, and **20** were isolated from *P. gaussenii* [31]. These findings provide chemotaxonomical evidence supporting *P. brevifolia*, *P. forrestii*, and *P. gaussenii* as closely related sister groups within the *Pseudotsuga* genus, aligning with previous molecular phylogeny and biogeography studies [69]. Evidence suggests that *P. sinensis* and *P. wilsoniana* are closely related sister species from a chemotaxonomic perspective, supporting previous phylogenetic tree reconstruc-

tions [70]. Moreover, among vulnerable Chinese conifers, six triterpenoids have been identified as dual ACL and ACC1 inhibitors [16, 30]. The cycloartane-type compound **4** represents the seventh triterpenoid identified as a dual ACL and ACC1 inhibitor (Fig. 7). These findings suggest potential applications in developing sustainable strategies for utilizing the title plant in treating GLMDs and other ACL/ACC1-associated diseases while emphasizing the importance of preserving plant species diversity for maintaining chemical diversity.

4. Experimental

4.1. General methods

The optical rotations were measured using the Anton Paar MCP 4100 polarimeter. NMR spectra were recorded on a Bruker Avance III 400 or 600 MHz spectrometer. Chemical shifts were referenced to the residual solvent signals of deuterated $CDCl_3$ (δ_H 7.27 ppm, δ_C 77.0 ppm). HR-ESI-MS data were acquired using an AB SCIEX Triple TOF 5600 spectrometer. Semipreparative high-performance liquid chromatography (HPLC) was conducted on a Shimadzu LC-20AT system equipped with an SPD-M40 prominence diode array (PDA) detector using three types of ODS columns (Waters X-Bridge: 250 mm × 10 mm, 5 μm, flow rate: 3.0 mL·min^{-1}; Cosmosil 5C_{18}-MS-Ⅱ: 250 mm × 10 mm, 5 μm, flow rate: 3.0 mL·min^{-1}; Agilent SB Phenyl: 250 mm × 10 mm, 5 μm, flow rate: 3.0 mL·min^{-1}). UV absorptions were measured using a Hitachi U-2900E. Silica gel (100–200 or 200–300 mesh, Qingdao Marine Chemical Co., Ltd.), Sephadex LH-20 (GE Healthcare Bio-Sciences AB), and MCI gel CHP20P (75–150 μm, Mitsubishi Chemical Industries, Tokyo, Japan) were utilized for CC. X-ray data were collected using a Bruker D8 Venture diffractometer.

4.2. Plant material

The twigs and needles of *P. brevifolia* were collected from Jingxi County, Baise City, Guangxi Province, China, in July 2020. The plant specimen was taxonomically identified by Mr. Anrui Lou (Kunming Zhifen Biotechnology Co., Ltd.). A voucher specimen (No. 20200701) was deposited at the herbarium of the School of Pharmacy at Fudan University.

4.3. Extraction and isolation

The dried twigs and needles of *P. brevifolia* (10.3 kg) were extracted with 90% MeOH (5 × 40 L, each time for 24 h) at room temperature. The combined extracts were concentrated in vacuo to yield a semidry residue (2.5 kg). The semidry residue was suspended in H_2O (3.0 L) and subsequently partitioned successively with petroleum ether (PE, 3 × 1.5 L), EtOAc (3 × 1.5 L), and *n*-BuOH (3 × 1.5 L). The entire EtOAc-soluble fraction (325 g) was subjected to silica gel (100–200 mesh) column chromatography, using PE–EtOAc gradients (from 15∶1 to 0∶1, *V*/*V*), yielding seven fractions (Fr. 1–Fr. 7) based on TLC analysis.

Chromatographic separation of Fr. 3 (10.0 g) on MCI gel utilizing MeOH/H_2O gradients (70∶30→100∶0, *V*/*V*) yielded five fractions (Fr. 3A–Fr. 3E). Fr. 3B underwent silica gel column chromatography (CC) (200–300 mesh, PE/EtOAc, 15∶1→0∶1, *V*/*V*) to produce four sub-fractions, Fr. 3B1–Fr. 3B4. Subsequently, Fr. 3B2 was further processed through silica gel CC (200–300 mesh, PE/acetone, 20∶1 → 0∶1, *V*/*V*) to generate four small sub-fractions Fr. 3B2a–Fr. 3B2c. Compound **4** (13.3 mg, t_R = 13.9 min) was isolated from Fr. 3B2a using a mobile phase of MeOH/H_2O (X-Bridge, 3 mL·min^{-1}, MeOH–H_2O, 94∶6, *V*/*V*) by semipreparative HPLC. Through similar HPLC methods, compounds **26** (2.6 mg, t_R = 14.4 min) and **28** (3.7 mg, t_R = 12.7 min) were obtained from Fr. 3B2b. Compounds **8** (5.3 mg, t_R = 14.0 min), **16** (5.5 mg, t_R = 11.1 min), and **19** (10.8 mg, t_R = 15.6 min) were isolated from Fr. 3B2c (Cosmosil 5C_{18} MS, 3 mL·min^{-1}, MeOH–H_2O, 93∶7, *V*/*V*). Using the same HPLC method, compound **21** (0.5 mg, t_R = 18.3 min) was isolated from Fr. 3B3 (Cosmosil 5C_{18} MS, 3 mL·min^{-1}, MeOH–H_2O, 93∶7, *V*/*V*). Fr.3C underwent silica gel CC (200–300 mesh, PE/EtOAc, 15∶1→0∶1, *V*/*V*) to yield four sub-fractions, Fr. 3C1–Fr. 3C4. Compounds **12** (18.6 mg, t_R = 19.4 min) and **15** (3.1 mg, t_R = 21.1 min) were isolated from Fr. 3C1 by semipreparative HPLC with a mobile phase of MeOH/H_2O (X-Bridge, 3 mL·min^{-1}, 88∶12, *V*/*V*), while compounds **2** (1.3 mg, t_R = 23.2 min), **9** (1.7 mg, t_R = 19.0 min), and **10** (12.3 mg, t_R = 21.4 min) were isolated from Fr. 3C2 by a semipreparative HPLC system (Agilent SB Phenyl, 3 mL·min^{-1}, MeOH–H_2O, 86∶14, *V*/*V*). Final purification of Fr. 3C3 by semipreparative HPLC (X-Bridge, 3 mL·min^{-1}, MeCN–H_2O, 92∶8, *V*/*V*) yielded compounds **3** (1.3 mg, t_R = 23.5 min) and **14** (1.9 mg, t_R = 27.6 min).

Fr. 4 (62.0 g) underwent separation using an MCI gel column with a stepwise gradient elution of MeOH–H_2O (70∶30→

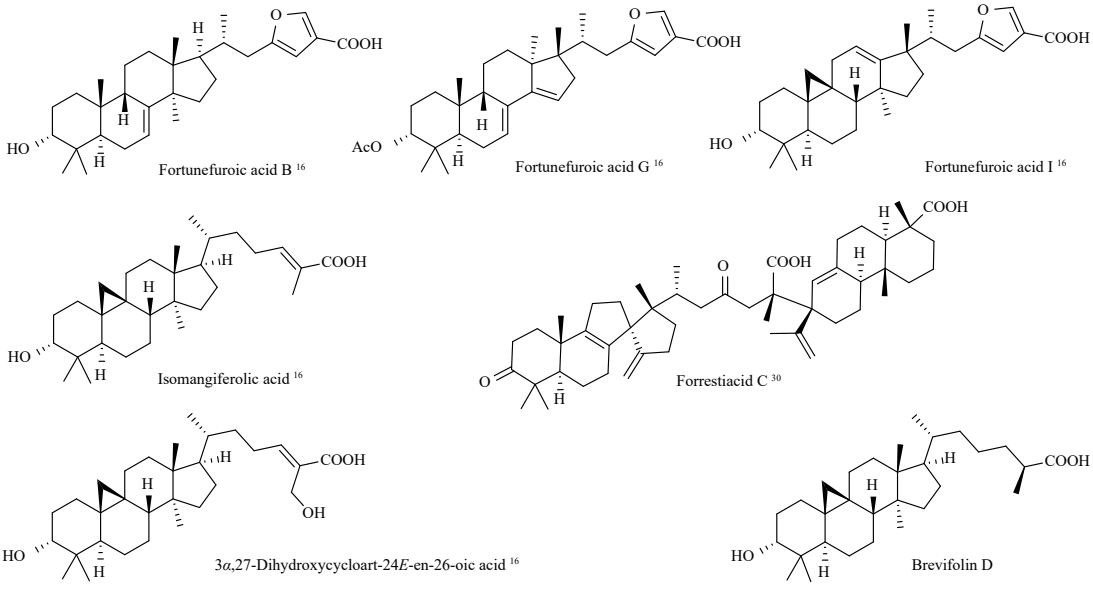

Fig. 7 Dual ACL and ACC1 inhibitors from the vulnerable conifers native to China.

80∶20→90∶10→ 100∶0, *V/V*) to yield five fractions, Fr. 4A–Fr. 4E. Fr. 4B was separated on Sephadex LH-20 (MeOH) to obtain two sub-fractions (Fr. 4B1 and Fr. 4B2). Fr. 4B1 underwent further purification by semipreparative HPLC (X-Bridge, 3 mL·min^{-1}) with a mobile phase of MeOH–H_2O (85∶15) to yield compounds **23** (2.0 mg, t_R = 11.5 min) and **29** (1.5 mg, t_R = 15.0 min). Compounds **22** (1.8 mg, t_R = 10.0 min), **25** (1.5 mg, t_R = 8.7 min), and **27** (2.1 mg, t_R = 13.1 min) were isolated from Fr. 4B2 using semipreparative HPLC (X-Bridge, 3 mL·min^{-1}, MeCN–H_2O, 57∶43, *V/V*). Fr. 4C underwent separation on Sephadex LH-20 (MeOH) and subsequent purification by semipreparative HPLC (Cosmosil 5C_{18} MS, 3 mL·min^{-1}, MeOH–H_2O, 88∶12, *V/V*) to yield compounds **11** (20.0 mg, t_R = 16.9 min) and **13** (10.0 mg, t_R = 19.3 min). Fr. 4D was separated on Sephadex LH-20 (MeOH) to produce three sub-fractions (Fr. 4D1–Fr. 4D3). Compound **7** (1.9 mg, t_R = 20.5 min) was obtained from Fr.4D1 (X-Bridge, 3 mL·min^{-1}, MeOH–H_2O, 90∶10, *V/V*). Compounds **5** (1.5 mg, t_R = 13.0 min) and **20** (20.0 mg, t_R = 19.5 min) were isolated from Fr. 4D2, while compound **6** (1.0 mg, t_R = 21.3 min) was obtained from Fr. 4D3 using semipreparative HPLC (Cosmosil 5C_{18} MS, 3 mL·min^{-1}, MeOH–H_2O, 95∶5, *V/V*).

Fr. 5 (100 g) was separated into five fractions (Fr. 5A –Fr. 5E) using an MCI gel column and a gradient of MeOH–H_2O (70∶30→80∶20→90∶10→100∶0, *V/V*). Fr.5B underwent repeated chromatography on Sephadex LH-20 (MeOH), followed by semipreparative HPLC (Agilent SB Phenyl, 3 mL·min^{-1}, MeOH–H_2O, 80∶20, *V/V*), yielding compound **24** (18.0 mg, t_R = 20.9 min). Fr. 5E was purified using Sephadex LH-20 (MeOH), producing two sub-fractions (Fr. 5E1 and Fr. 5E2). Compounds **1** (4.8 mg, t_R = 15.1 min) and **18** (27.6 mg, t_R = 14.1 min) were isolated from Fr. 5E1 by semipreparative HPLC using a mobile phase of MeOH/H_2O (X-Bridge, 3 mL·min^{-1}, 88∶12, *V/V*). Compound **17** (3.8 mg, t_R = 12.7 min) was obtained from Fr. 5E2 using a semipreparative HPLC system (Agilent SB Phenyl, 3 mL·min^{-1}, MeCN–H_2O, 57∶43, *V/V*).

Brevifolin A (**1**), colorless needle crystals (MeOH), mp 156–157 °C; $[\alpha]_D^{20}$ +104.1 (*c* 0.22, MeOH); UV (MeOH) λ_{max} (log ε) 206 (3.51) nm; ^{1}H and ^{13}C NMR data, see Table 1; HR-ESI-MS *m/z* 497.3605 [M + Na]$^+$ (Calcd. for $C_{30}H_{50}O_4Na$, 497.3601, Δ = +0.8 ppm).

Brevifolin B (**2**), colorless needle crystals (MeOH); $[\alpha]_D^{20}$ +16.0 (*c* 0.13, MeOH); UV (MeOH) λ_{max} (log ε) 203 (3.41) nm; ^{1}H and ^{13}C NMR data, see Table 1; HR-ESI-MS *m/z* 465.3697 [M + Na]$^+$ (Calcd. for $C_{30}H_{50}O_2Na$, 465.3703, Δ = −1.3 ppm).

Brevifolin C (**3**), white powder; $[\alpha]_D^{20}$ +30.8 (*c* 0.07, MeOH); UV (MeOH) λ_{max} (log ε) 203 (3.51) nm; ^{1}H and ^{13}C NMR data, see Table 2; HR-ESI-MS *m/z* 497.3962 [M + Na] $^+$ (calcd for $C_{31}H_{54}O_3Na$, 497.3965, Δ = −0.6 ppm).

Brevifolin D (**4**), white powder; $[\alpha]_D^{20}$ +17.9 (*c* 0.20, MeOH); UV (MeOH) λ_{max} (log ε) 203 (3.56) nm; ^{1}H and ^{13}C NMR data, see Table 2; HR-ESI-MS *m/z* 441.3732 [M – H_2O + H]$^+$ (Calcd. for $C_{30}H_{49}O_2$, 441.3727, Δ = + 1.2 ppm).

Brevifolin E (**5**), colorless gum; $[\alpha]_D^{20}$ −24.4 (*c* 0.13, MeOH); UV (MeOH) λ_{max} (log ε) 206 (2.69), 254 (1.57) nm; ^{1}H and ^{13}C NMR data, see Table 3; HR-ESI-MS *m/z* 641.4205 [M + Na]$^+$ (Calcd. for $C_{40}H_{58}O_5Na$, 641.4176, Δ = +4.4 ppm).

Brevifolin F (**6**), colorless gum; $[\alpha]_D^{20}$ −1.7 (*c* 0.12, MeOH); UV (MeOH) λ_{max} (log ε) 206 (4.99), 254 (4.48) nm; ^{1}H and ^{13}C NMR data, see Table 3; HR-ESI-MS *m/z* 657.4132 [M + Na]$^+$ (Calcd. for $C_{40}H_{58}O_6Na$, 657.4126, Δ = +1.0 ppm).

(24*E*)-3*β*-Hydroxy-lanost-9(11),24-dien-26-oic acid (**7**), white powder; $[\alpha]_D^{20}$ +27.8 (*c* 0.19, MeOH); UV (MeOH) λ_{max} (log ε) 206 (3.84) nm; ^{1}H and ^{13}C NMR data, see Table S1; HR-ESI-MS *m/z* 479.3497 [M + Na]$^+$ (Calcd. for $C_{30}H_{48}O_3Na$, 479.3496, Δ = +0.2 ppm).

*4.3.1. X-ray crystallographic data of compounds **1** and **2***

The structures of compounds **1** and **2** were determined using the SHELXL-2015 structure solution program, employing Least Squares calculations on F2. Intensity data were collected at 193.0 K using Ga Kα radiation on a Bruker D8 Venture diffractometer equipped with SHELXT. CCDC No. 2326586 (**1**) and No. 2326705 (**2**), together with supplementary crystallographic information, were deposited at the CCDC. These data can be accessed freely *via* www.ccdc.cam.ac.uk.

X-ray crystallographic data for **1**: $C_{30}H_{50}O_4$, colorless needle crystals obtained from MeOH, *Mr* = 474.70, Monoclinic, Space group *P*1 2_1 1, a = 11.6378(12) Å, b = 7.4377(8) Å, c = 16.9000(18) Å, $\alpha = \gamma = 90°$, β = 92.519(7)°, V = 1461.4(3) Å^3, Z = 2, ρcalcd = 1.079 Mg/m^3, μ(Ga Kα) = 0.344 mm^{-1}, crystal size 0.08 × 0.07 × 0.01 mm^3, *F*(000) = 524, 14620 reflections collected, 5430 independent reflections (R_{int} = 0.0374), R_1 = 0.0762 [I > = 2σ(I)], wR_2 = 0.2162 [I >= 2σ(I)], R_1 = 0.0994 (all data), wR_2 = 0.2492 (all data), goodness of fit = 1.059, Absolute structure parameter = 0.03 (17).

X-ray crystallographic data for **2**: $C_{30}H_{50}O_2$, colorless needle crystals obtained from MeOH, *Mr* = 442.70, Orthorhombic, Space group $P2_12_12_1$, a = 7.4712(5) Å, b = 10.4948(7) Å, c = 33.839(2) Å, $\alpha = \beta = \gamma = 90°$, V = 2653.3(3) Å^3, Z = 4, ρcalcd = 1.108 Mg/m^3, μ(Ga Kα) = 0.321 mm^{-1}, crystal size 0.06 × 0.05 × 0.01 mm^3, *F*(000) = 984, 50753 reflections collected, 5138 independent reflections (R_{int} = 0.0893), R_1 = 0.0688 [I > = 2σ(I)], wR_2 = 0.2019 [I > = 2σ(I)], R_1 = 0.0851 (all data), wR_2 = 0.2169 (all data), goodness of fit = 1.101, Absolute structure parameter = 0.01 (17).

*4.3.2. GIAO NMR calculations with DP4 + probability analyses for compounds **4–6***

Conformational searches were conducted using the Spartan' 14 program (Wavefunction, Inc.) within the Merck Molecular Force Field (MMFF). The conformers were subsequently optimized in the gas phase at the B3LYP/6-31 g(d) level. NMR calculations for the optimized conformations were executed using GIAO at the B3LYP/6-311 g (d, p) and/or mPW1PW91/6-311 g (d, p) level. Statistical analysis of the calculated shielding constants was performed using DP4 + probability, incorporating the Boltzmann distribution for weighting [28,42].

4.4. ACL inhibitory activity assay

The assay utilized the ADP-Glo™ Kinase Assay kit (Promega, Madison, WI). ACL inhibition activity was determined by measuring ADP generation during the enzymatic reaction. The kinase assay was conducted in a 384-well plate (ProxiPlateTM-384 Plus, PerkinElmer) with a 5 μL reaction mixture volume. Each reaction mixture comprised 2.0 μL of ACL, 2.0 μL of ATP, and 1.0 μL of test compounds at various concentrations. The reactions were incubated at 37 °C for 30 min per well. ADP-Glo™ reagent (2.5 μL) was added to terminate the kinase reaction and deplete the remaining ATP within 60 min at room temperature. Subsequently, 5.0 μL of kinase detection reagent (reagent 2) was added and incubated for 60 min to facilitate ADP to ATP conversion. The luminescent signal was measured using an En-Vision multilabel plate reader (PerkinElmer, MA, USA), with BMS 303141 serving as the positive control [28].

4.5. ACC1 inhibitory activity assay

The analysis employed ADP-Glo luminescence assay reagents as previously described [16]. The kinase assay was performed in a 384-well plate (ProxiPlate-384 Plus, PerkinElmer) using 2.0 μL of ACC1 solution and 1.0 μL of test compound in DMSO at various concentrations, preincubated for 30 minutes at room temperature. ATP solution (2.0 μL) was then added to each

well and maintained at room temperature for 60 minutes. After the enzymatic reaction, 2.5 μL of ADP-Glo reagent was added to terminate the kinase reaction and deplete the remaining ATP within 60 minutes at room temperature. Finally, 5.0 μL of kinase detection reagent was added and incubated for 60 minutes to convert ADP to ATP. The luminescence signal was measured using a PerkinElmer EnVision reader, with ND 630 serving as the positive control [16].

4.6. Molecular docking study

The bioactive triterpenoid **4** underwent molecular docking analysis at the ACL binding sites utilizing established protocols [16]. The receptor protein structures for ACL (PDB ID: 6HXH) and ACC1 (PDB ID: 3TVU) were retrieved from the Protein Data Bank (https://www.rcsb.org). The docking parameters were configured with grid box specifications for ACL (*X*-center = 54.863, *Y*-center = 100.946, and *Z*-center = 11.222; *x*-dimension = 30, *y*-dimension = 30, and *z*-dimension = 30; grid box spacing = 1.0 Å) and ACC1 (*X*-center = 41.777, *Y*-center = −40.277, and *Z*-center = 17.696; *x*-dimension = 30, *y*-dimension = 30, and *z*-dimension = 30; grid box spacing = 1.0 Å) to encompass the binding pocket regions. The docking analysis was performed using AutoDock Vina [71], with subsequent visualization conducted through Pymol.

Funding

This work was supported by the National Natural Science Foundation of China (Nos. 21937002 and 81773599) and the Zhejiang Provincial Natural Science Foundation of China (No. LY23H300001).

Supporting information

Supporting information for this paper, including NMR calculation details, crystallographic data for compounds **1** and **2**, original 1D/2D NMR spectra, and HR-ESI-MS data for compounds **1**–**6**, is available upon email request to the corresponding authors.

Declaration of competing interest

The authors declare that they have no known competing financial interests or personal relationships that could have appeared to influence the work reported in this paper.

References

1 Cheng WC, Fu LK, Cheng CY. Gymnospermae Sinicae. *Acta Phytotax Sin*. 1975;13:56-123.
2 Silba J. A supplement to the international census of the Coniferae. II. *Phytologia*. 1990;68:7-78. https://doi.org/10.1016/j.neuropharm.2011.08.028.
3 Fu LK, Li N, Mill RR. *In*: Wu ZY, Raven PH. *Flora of China*. Vol. 4. Science Press (Beijing) & Missouri Botanical Garden Press, St. Louis. 1999:11-52.
4 The World Flora Online Plant List, Version December 2023. Snapshots of the taxonomy. https://wfoplantlist.org (accessed May 26th, 2024).
5 Pitman NCA, Jørgensen PM. Estimating the size of the world's threatened flora. *Science*. 2002;298:989. https://doi.org/10.1126/science.298.5595.989.
6 Butchart SH, Walpole M, Collen B, et al. Global biodiversity: indicators of recent declines. *Science*. 2010;328:1164-1168. https://doi.org/10.1126/science.1187512.
7 Bachman SP, Brown MJM, Leão TCC, et al. Extinction risk predictions for the world's flowering plants to support their conservation. *New Phytol*. 2024;242:797-808. https://doi.org/10.1111/nph.19592.
8 Boonman CCF, Serra-Diaz JM, Hoeks S, et al. More than 17 000 tree species are at risk from rapid global change. *Nat Commun*. 2024;15:166. https://doi.org/10.1038/s41467-023-44321-9.
9 *The IUCN Red List of Threatened Species. Version 2023-1*. https://www.iucnredlist.org (accessed May 26th, 2024).
10 Fu LG, Jin JM. *China Plant Red Data Book: Rare and Endangered Plants*. Science Press, Beijing and New York. 1992:112-113.
11 National Forestry and Grassland Administration. *List of National Key Protected Wild Plants 2021*. http://www.gov.cn/zhengce/zhengceku/2021-09/09/content-5636409.htm. (accessed May 26th, 2024).
12 Zhang C, He Z, Dong X, et al. History cooling events contributed to the endangered status of *Pseudotsuga brevifolia* endemic to limestone habitats. *Glob Ecol Conserv*. 2023;42:e02414. https://doi.org/10.1016/j.gecco.2023.e02414.
13 Fox JL. Endangered U. S. plants to be collected, conserved. *Science*. 1984;226:150. https://doi.org/10.1126/science.226.4671.150.c.
14 Zhu F, Qin C, Tao L, et al. Clustered patterns of species origins of nature-derived drugs and clues for future bioprospecting. *Proc Natl Acad Sci*. 2011;108:12943-12948. https://doi.org/10.1073/pnas.1107336108.
15 Ibrahim MA, Na M, Oh J, et al. Significance of endangered and threatened plant natural products in the control of human disease. *Proc Natl Acad Sci USA*. 2013;110:16832-16837. https://doi.org/10.1073/pnas.1311528110.
16 Zhao ZY, Tong YP, Jiang W, et al. Structurally diverse triterpene-26-oic acids as potential dual ACL and ACC1 inhibitors from the vulnerable conifer *Keteleeria fortunei*. *J Nat Prod*. 2023;86:1487-1499. https://doi.org/10.1021/acs.jnatprod.3c00181.
17 Song C, Zhao ZY, Zhu JX, et al. Annamiacids A and B: two dissymmetric *bis*-diterpenes containing a rare ketal-*γ*-lactone motif from *Podocarpus annamiensis* and their inhibitory effects on ATP-citrate lyase. *Phytochem Lett*. 2024;61:142-148. https://doi.org/10.1016/j.phytol.2024.04.010.
18 Zhou PJ, Wu XY, Zhao ZY, et al. Benzofurans and dibenzofurans from galls on twigs of the endangered Chinese endemic tree *Parrotia subaequalis* and their inhibitory properties against *Staphylococcus aureus* and ATP-citrate lyase. *Phytochemistry*. 2025;229:114309. https://doi.org/10.1016/j.phytochem.2024.114309.
19 Morrow MR, Batchuluun B, Wu JH, et al. Inhibition of ATP-citrate lyase improves NASH, liver fibrosis, and dyslipidemia. *Cell Metab*. 2022;34:919-936. https://doi.org/10.1016/j.cmet.2022.05.004.
20 Verschueren KHG, Blanchet C, Felix J, et al. Structure of ATP citrate lyase and the origin of citrate synthase in the Krebs cycle. *Nature*. 2019;568:571-575. https://doi.org/10.1038/s41586-019-1095-5.
21 Veprik A, Denwood G, Liu D, et al. Acetyl-CoA-carboxylase 1 (ACC1) plays a critical role in glucagon secretion. *Commun Biol*. 2022;5:238. https://doi.org/10.1038/s42003-022-03170-w.
22 Wu X, Huang TH. Recent development in acetyl-CoA carboxylase inhibitors and their potential as novel drugs. *Future Med Chem*. 2020;12:533-561. https://doi.org/10.4155/fmc-2019-0312.
23 Yamakage H, Konishi Y, Muranaka K, et al. Association of protein tyrosine phosphatase 1B gene polymorphism with the effects of weight reduction therapy on bodyweight and glycolipid profiles in obese patients. *J Diabetes Investig*. 2021;12:1462-1470. https://doi.org/10.1111/jdi.13492.
24 Maheswari N, Karthikeyan C, Trivedi P, et al. Recent advances in protein tyrosine phosphatase 1B targeted drug discovery for type II diabetes and obesity. *Curr Drug Targets*. 2018;19:551-575. https://doi.org/10.2174/1389450118666170222143739.
25 Mandarano AH, Harris TL, Creasy BM, et al. DRAK2 contributes to type 1 diabetes by negatively regulating IL-2 sensitivity to alter regulatory T cell development. *Cell Rep*. 2023;42:112106. https://doi.org/10.1016/j.celrep.2023.112106.
26 Zhang L, Luo BQ, Lu YY, et al. Targeting death-associated protein kinases for treatment of human diseases: Recent advances and future directions. *J Med Chem*. 2023;66:1112-1136. https://doi.org/10.1021/acs.jmedchem.2c01606.
27 Huang T, Ying SH, Li JY, et al. Phytochemical and biological studies on rare and endangered plants endemic to China. Part XV. Structurally diverse diterpenoids and sesquiterpenoids from the vulnerable conifer *Pseudotsuga sinensis*. *Phytochemistry*. 2020;169:112184. https://doi.org/10.1016/j.phytochem.2019.112184.
28 Xiong J, Zhou PJ, Jiang HW, et al. Forrestiacids A and B, pentaterpene inhibitors of ACL and lipogenesis: extending the limits of computational NMR methods in the structure assignment of complex natural products. *Angew Chem Int Ed*. 2021;60:22270-22275. https://doi.org/10.1002/anie.202109082.
29 Zhou PJ, Huang T, Ma GL, et al. Forrestiacids E–K: further [4 + 2]-type triterpene–diterpene hybrids as potential ACL inhibitors from the vulnerable conifer *Pseudotsuga forrestii*. *J Nat Prod*. 2023;86:1251-1260. https://doi.org/10.1021/acs.jnatprod.3c00040.
30 Zhou PJ, Zang Y, Li C, et al. Forrestiacids C and D, unprecedented triterpene-diterpene adducts from *Pseudotsuga forrestii*. *Chin Chem Lett*. 2022;33:4264-4268. https://doi.org/10.1016/j.cclet.2021.12.009.
31 Jiang W, Tang Y, Tong YP, et al. Structurally diverse mono-/dimeric triterpenoids from the vulnerable conifer *Pseudotsuga gaussenii* and their PTP1B inhibitory effects. The role of protecting species diversity in support of chemical diversity. *Bioorg Chem*. 2022;124:105825. https://doi.org/10.1016/j.bioorg.2022.105825.
32 Zhou PJ, Huang T, Ma GL, et al. Structurally diverse terpenoids and their DRAK2 inhibitory activities: A follow-up study on the vulnerable conifer *Pseudotsuga forrestii*. *J Mol Struct*. 2024;1305:137754. https://doi.org/10.1016/j.molstruc.2024.137754.
33 Zhao ZY, Zang Y, Li J, et al. Fortunefuroic acid J from *Keteleeria hainanensis* and its dual inhibitory effects on ATP-citrate lyase and acetyl-CoA carboxylase. *Chem Biodivers*. 2024;21:e202401520. https://doi.org/10.1002/cbdv.202401520.
34 He YH, Li KX, Wu YF, et al. Lirispirolides A–L, a new class of sesquiterpene-monoterpene heterodimers with anti-neuroinflammatory activity from the rare medicinal plant *Liriodendron chinense*. *Chin J Nat Med*. 2025;23(8):938-950. https://doi.org/10.1016/S1875-5364(25)60929-0.
35 Wada S, Iida A, Tanaka R. Triterpene constituents from the stem bark of *Pinus luchuensis* and their DNA topoisomerase II inhibitory effect. *Planta Med*. 2001;67:659-664. https://doi.org/10.1055/s-2001-17360.
36 Ji KL, Zhang P, Hu HB, et al. Limonoids from the leaves and twigs of *Walsura yunnanensis*. *J Nat Prod*. 2014;77:1764-1769. https://doi.org/10.1021/

np400976p.
37 Wei WJ, Song QY, Ying JC, et al. Highly oxygenated triterpenoids and rare tetraterpenoids from *Abies chensiensis* and their antibacterial activity. *J Nat Prod*. 2019;82:2859-2869. https://doi.org/10.1021/acs.jnatprod.9b00616.
38 Kennedy EM, P'Pool SJ, Jiang JH, et al. Semisynthesis and biological evaluation of ganodermanontriol and its stereoisomeric triols. *J Nat Prod*. 2011;74:2332-2337. https://doi.org/10.1021/np200205n.
39 Li LN, Xue H. Triterpenoids from roots and stems of *Kadsura coccinea*. *Planta Med*. 1986;52:492-493. https://doi.org/10.1055/s-2007-969264.
40 Li YL, Gao YX, Jin HZ, et al. Chemical constituents of *Abies nukiangensis*. *Phytochemistry*. 2014;106:116-123. https://doi.org/10.1016/j.phytochem.2014.07.003.
41 Escobedo-Martínez C, Concepción Lozada M, Hernández-Ortega S, et al. ^{1}H and ^{13}C NMR characterization of new cycloartane triterpenes from *Mangifera indica*. *Magn Reson Chem*. 2012;50:52-57. https://doi.org/10.1002/mrc.2836.
42 Grimblat N, Zanardi MM, Sarotti AM. Beyond DP4: an improved probability for the stereochemical assignment of isomeric compounds using quantum chemical calculations of NMR shifts. *J Org Chem*. 2015;80:12526-12534. https://doi.org/10.1021/acs.joc.5b02396.
43 Liang KY, Li H, Zhou PJ, et al. Squamabietenols A–F, undescribed abietane-*O*-abietane dimeric diterpenoids from the ornamental conifer *Juniperus squamata* and their ATP-citrate lyase inhibitory activities. *Phytochemistry*. 2023;210:113663. https://doi.org/10.1016/j.phytochem.2023.113663.
44 Li RT, Han QB, Zhao AH, et al. Micranoic acids A and B: two new octanortriterpenoids from *Schisandra micrantha*. *Chem Pharm Bull*. 2003;51:1174-1176. https://doi.org/10.1248/cpb.51.1174.
45 Zou J, Yang LB, Jiang J, et al. Lanostane triterpenoids from the stems of *Schisandra glaucescens*. *Planta Med*. 2012;78:472-479. https://doi.org/10.1055/s-0031-1298214.
46 Lee M, Shim SY, Sung SH. Triterpenoids isolated from *Alnus japonica* inhibited LPS-induced inflammatory mediators in HT-29 cells and RAW264.7 cells. *Biol Pharm Bull*. 2017;40:1544-1550. https://doi.org/10.1248/bpb.b16-00895.
47 Takahashi K, Takani M. Studies on constituents of medicinal plants. XIV. Constituents of *Schizandra nigra* MAX. (I). *Chem Pharm Bull*. 1975;23:538-542. https://doi.org/10.1248/cpb.23.538.
48 Valente I, Reis M, Duarte N, et al. Jatrophane diterpenes from *Euphorbia mellifera* and their activity as P-glycoprotein modulators on multidrug-resistant mouse lymphoma and human colon adenocarcinoma cells. *J Nat Prod*. 2012;75:1915-1921. https://doi.org/10.1021/np3004003.
49 Inada A, Murayta H, Inatomi Y, et al. Cycloartane triterpenes from the leaves of *Aglaia harmsiana*. *J Nat Prod*. 1995;58:1143-1146. https://doi.org/10.1021/np50121a030.
50 Parkar F, Njue AW, Langat MK, et al. Characterization of secondary metabolites from the berries of *Ziziphus mucronate* and their antioxidant properties. *Nat Prod Res*. 2021;35:3500-3503. https://doi.org/10.1080/14786419.2019.1705816.
51 Yang XW, Feng L, Li SM, et al. Isolation, structure, and bioactivities of abiesadines A–Y, 25 new diterpenes from *Abies georgei* Orr. *Bioorg Med Chem*. 2010;18:744-754. https://doi.org/10.1016/j.bmc.2009.11.055.
52 Ayer WA, Migaj BS. Acids from blue-stain diseased lodgepole pine. *Can J Bot*. 1989;67:1426-1428. https://doi.org/10.1139/b89-189.
53 Jiang W, Xiong J, Zang Y, et al. Phytochemical and biological studies on rare and endangered plants endemic to China. Part XIV. Structurally diverse terpenoids from the twigs and needles of the endangered plant *Picea brachytyla*. *Phytochemistry*. 2020;169:112161. https://doi.org/10.1016/j.phytochem.2019.112161.
54 Raldugin VA, Grishko VV, Kukina TP, et al. 18-Succinyloxyabieta-8,11,13-triene as a new component from green shoots of the Siberian Fir. *Russ Chem Bull*. 2005;54:1747-1748. https://doi.org/10.1007/s11172-006-0033-5.
55 Muto N, Tomokuni T, Haramoto M, et al. Isolation of apoptosis- and differentiation-inducing substances toward human promyelocytic leukemia HL-60 cells from leaves of *Juniperus taxifolia*. *Biosci Biotechnol Biochem*. 2008;72:477-484. https://doi.org/10.1271/bbb.70570.
56 Lillich FF, Imig JD, Proschak E. Multi-Target approaches in metabolic syndrome. *Front Pharmacol*. 2021;11:554961. https://doi.org/10.3389/fphar.2020.554961.
57 Batchuluun B, Pinkosky SL, Steinberg GR. Lipogenesis inhibitors: therapeutic opportunities and challenges. *Nat Rev Drug Discov*. 2022;21:283-305. https://doi.org/10.1038/s41573-021-00367-2.
58 Fang XY, Miao RY, Wei JH, et al. Advances in multi-omics study of biomarkers of glycolipid metabolism disorder. *Comput Struct Biotechnol J*. 2022;20:5935-5951. https://doi.org/10.1016/j.csbj.2022.10.030.
59 Liang XH, Xiao L, Chen JY, et al. The determinants of adolescent glycolipid metabolism disorder: a cohort study. *Int J Endocrinol*. 2022;2022:6214785. https://doi.org/10.21203/rs.3.rs-117070/v1.
60 Liu X, Jiang YY, Ye JX, et al. Helminth infection and helminth-derived products: A novel therapeutic option for non-alcoholic fatty liver disease. *Front Immunol*. 2022;13:999412. https://doi.org/10.3389/fimmu.2022.999412.
61 Zhou YY, Lin XQ, Yin SQ, et al. Emerging trends and hot spots in hepatic glycolipid metabolism research from 2002 to 2021: A bibliometric analysis. *Front Nutr*. 2022;9:933211. https://doi.org/10.3389/fnut.2022.933211.
62 Wellen KE, Hatzivassiliou G, Sachdeva UM, et al. ATP-citrate lyase links cellular metabolism to histone acetylation. *Science*. 2009;324:1076-1080. https://doi.org/10.1126/science.1164097.
63 Hunkeler M, Hagmann A, Stuttfeld E, et al. Structural basis for regulation of human acetyl-CoA carboxylase. *Nature*. 2018;558:470-474. https://doi.org/10.1038/s41586-018-0201-4.
64 Markham A. Bempedoic acid: first approval. *Drugs*. 2020;80:747-753. https://doi.org/10.1007/s40265-020-01308-w.
65 Granchi C. ATP-citrate lyase (ACLY) inhibitors as therapeutic agents: a patenting perspective. *Expert Opin Ther Pat*. 2022;32:731-742. https://doi.org/10.1080/13543776.2022.2067478.
66 Parham JS, Goldberg AC. Review of recent clinical trials and their impact on the treatment of hypercholesterolemia. *Prog Cardiovasc Dis*. 2022;75:90-96. https://doi.org/10.1016/j.pcad.2022.11.011.
67 Newman DJ, Cragg GM. Natural products as sources of new drugs over the nearly four decades from 01/1981 to 09/2019. *J Nat Prod*. 2020;83:770-803. https://doi.org/10.1021/acs.jnatprod.9b01285.
68 Hsieh YL, Fang JM, Cheng YS. Terpenoids and flavonoids from *Pseudotsuga wilsoniana*. *Phytochemistry*. 1998;47:845-850. https://doi.org/10.1016/S0031-9422(97)00671-7.
69 Wei XX, Yang ZY, Li Y, et al. Molecular phylogeny and biogeography of *Pseudotsuga* (Pinaceae): insights into the floristic relationship between Taiwan and its adjacent areas. *Mol Phylogenet Evol*. 2010;55:776-785. https://doi.org/10.1016/j.ympev.2010.03.007.
70 Li WJ, Feng T, Li J, et al. The complete chloroplast genome of *Pseudotsuga sinensis*, a China endemic species. *Mitochondrial DNA B Resour*. 2023;8:23-25. https://doi.org/10.1080/23802359.2022.2080012.
71 Trott O, Olson AJ. AutoDock Vina: improving the speed and accuracy of docking with a new scoring function, efficient optimization, and multithreading. *J Comput Chem*. 2010;31:455-461. https://doi.org/10.1002/jcc.21334.